ACS APPLIED MATERIALS & INTERFACES

Research Article

www.acsami.org

Electrochemical Performance of Electrospun Free-Standing Nitrogen-Doped Carbon Nanofibers and Their Application for Glucose Biosensing

Dong Liu,[†] Xueping Zhang,[†,‡] and Tianyan You*[,†]

[†]State Key Laboratory of Electroanalytical Chemistry, Changchun Institute of Applied Chemistry, Chinese Academy of Sciences, 5625 Renmin Street, Changchun 130022, China

[‡]University of Chinese Academy of Sciences, 19A Yuquan Road, Beijing 100049, China

Supporting Information

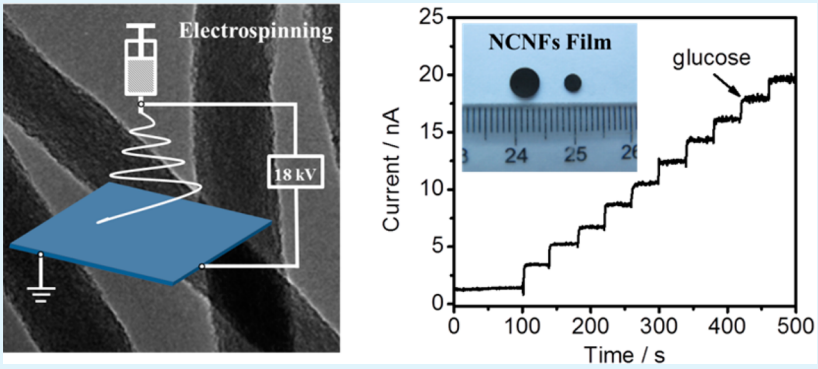

ABSTRACT: In spite of excellent electrochemical properties, nitrogen-doped carbon nanofibers (NCNFs) have rarely been studied in the field of electroanalysis. In this work, we investigated the electrochemical properties and biosensing performance of NCNFs prepared by a newly proposed approach. The as-obtained NCNFs present a unique free-standing structure with high flexibility which could be convenient for electrode modification. Electrochemical measurements of typical redox species including $[Ru(NH_3)_6]^{3+/2+}$, $[Fe(CN)_6]^{3-/4-}$, $[Fe(H_2O)_6]^{3+/2+}$, and dopamine indicate that the NCNFs have a larger surface area and faster electron transfer rate compared with carbon nanofibers (CNFs). The presence of high content of pyrrolic-N and abundant defective sites in NCNFs leads to an obvious positive shift of peak potential for oxygen reduction at NCNFs relative to that obtained at CNFs. The unique structure and properties greatly enhance the electrochemical performance of NCNFs. The glucose biosensor based on glucose oxidase/NCNFs shows linear ranges of 0.2−1.2 mM at −0.42 V and 0.05−3 mM at 0.40 V both with high stability. These results suggest that the NCNFs could be a convenient and stable platform for electrochemical biosensors.

KEYWORDS: *electrochemistry, free-standing structure, nitrogen-doped carbon nanofibers, glucose biosensing*

1. INTRODUCTION

Carbon materials are widely employed for the electrochemical analysis of biomolecules and catalyst support owing to their advantageous properties, including low cost, wide potential window, and high stability.[1−5] Among these studies, many reports aimed at the construction of state-of-the-art electrochemical biosensors with excellent electroanalytical performance.[6−10] However, the relatively inert electrochemical activity and poor biocompatibility of pristine carbon nanomaterials have limited their applications, and many methods are developed to solve these issues.[4,11,12]

Doping the heteroatom into the nanomaterials has been verified to be a feasible approach for the modulation of host properties.[13,14] As for carbons, the inclusion of electron-accepting nitrogen atoms, which could form valence bonds with adjacent carbon atoms and improve their electron-donor ability, may enhance the properties of bulk carbon nanomaterials, such as electrocatalytic activity toward oxygen reduction reaction.[15−17] More recently, nitrogen-doped carbon nanomaterials are extensively investigated in biosensors for their favorable biocompatibility and sensitivity.[18−20] For example, Kamata et al. have synthesized a novel nitrogen-doped carbon film via electron cyclotron resonance sputtering which could be used for the highly sensitive biosensing of DNA bases.[21] The major forms of these nanomaterials are powder and flake; however, nitrogen-doped carbon nanomaterials with free-standing structure could be more attractive in the fabrication of biosensors for their unique electrochemical properties and excellent processability. In fact, previous studies demonstrate that the free-standing films, such as the graphene−TiO_2 hybrid

Received: October 5, 2013
Accepted: April 8, 2014
Published: April 8, 2014

paper, and mesoporous carbon thin films could provide a continuous electron transport framework with lower ion transport resistance, shorter electrolyte diffusion length, and higher active material-to-substrate mass ratios in comparison with conventional nanomaterials.[22−24] Unfortunately, the investigation of free-standing nanomaterials in electroanalysis has been seriously limited by the relatively complex preparation procedures.

Electrospun carbon nanofibers (CNFs) have been considered as an ideal platform for electrochemical measurements owing to the free-standing structure and low background noise.[25] Additionally, the preparation of CNFs via electrospinning combined with thermal treatment is simple and efficient. Nevertheless, nitrogen-doped CNFs (NCNFs) are usually prepared via chemical vapor deposition or post-treatment under a flow of ammonia (NH_3) which may need high skill and fine manipulation.[26,27] In addition, there are rarely reports concerning the application of NCNFs in electrochemical analysis despite their promising development. Hence, it is desirable to develop a simple method to prepare NCNFs for the investigations in biosensors.

Herein, we developed a simple strategy for the production of electrospun free-standing NCNF film and further studied the electrochemical properties of NCNFs. The obtained NCNFs exhibit an average diameter of 146 nm with rough surface according to SEM and TEM. XPS results reveal that 42 at. % of nitrogen is in the form of pyrrolic-N for NCNFs, much higher than that for CNFs. A high content of pyrrolic-N combined with abundant defective sites leads to the fast electron transfer rate and high oxygen reduction activity at NCNFs. For the unique free-standing structure and high flexibility of NCNF film, the NCNF-based glucose biosensor could be conveniently fabricated, which exhibits fast response and high stability toward glucose detection.

2. EXPERIMENTAL SECTION

2.1. Materials and Reagents. Polyacrylonitrile (PAN, average M_w 150 000), ammonium iron(II) sulfate hexahydrate (≥98%), hexaamineruthenium chloride (≥98%), glucose oxidase (GOx, from *Aspergillus niger*, 185 units mg^{-1}), glucose (≥99.5%), dopamine hydrochloride (DA), uric acid (UA, ≥99%), and ascorbic acid (AA, ≥99%) were purchased from Sigma-Aldrich. Potassium ferricyanide (≥99.5%) and dimethylfomamide (DMF, ≥99.5%) were obtained from Beijing Chemical Co. (China).

2.2. Apparatus. The scanning electron microscopy (SEM) images were obtained using a PHILIPS XL-30 ESEM with an accelerating voltage of 20 kV. The transmission electron microscopy (TEM) images and high-resolution TEM (HRTEM) were acquired on a TECNAI G2 with the accelerating voltage of 200 kV. X-ray photoelectron spectroscopy (XPS) was performed on a Thermo ESCALAB 250 with Al Kα radiation (pass energy, 20.0 eV; energy step size. 1.0 eV; total acq. time: 1 min 0.1 s). Raman spectra were performed on Renishaw RM-1000 with a laser excitation of 514.5 nm. Electrochemical impedance spectroscopy (EIS) was performed on an AUTOLAB PGSTAT302N in 5 mM $[Fe(CN)_6]^{3-/4-}$ with 0.5 M KCl as supporting electrolyte within the frequency range of $0.01-10^5$ Hz. All other electrochemical measurements were performed on a CHI 832C electrochemical workstation (Shanghai, China).

2.3. Preparation of NCNFs. The NCNFs were prepared by the carbonization of electrospun PAN nanofibers, and the preparation process of PAN nanofibers was similar to our previous work.[13] Briefly, 10 wt % PAN solution was prepared by dissolving 0.5229 g of PAN in DMF as the electrospun solution. The electrospinning process was carried out in the electric fields of 100 kV/m with a flow rate of 1.0 mL/h. Stabilization and carbonization were performed by the following steps: (1) stabilized at 300 °C for 60 min in air, (2) heated to 900 °C and kept for 120 min in nitrogen, (3) cooled to room temperature in nitrogen. The entire thermal treatment procedure was performed with a heating rate of 10 °C/min. An enclosed device comprised by two combustion boats was employed as the reactor for PAN nanofibers to increase the resident time of tail gas in it during the high-temperature process. The pristine CNFs were prepared via the same procedure in one combustion boat except the first step which was stabilized in air.

2.4. Fabrication of GOx/NCNF-Modified Electrodes. The NCNF film was cut to a disk shape with a diameter of 2 mm and directly adhered to the surface of the glassy carbon electrode (NCNFs/GCE). Amounts of 2 μL of GOx solution (2 mg/mL) and 1 μL of 0.5 wt % nafion solution were casted successively on the surface of NCNFs/GCE and then dried at 4 °C. Finally, the modified electrode was immersed in PBS to remove the loosely adsorbed GOx and was stored at 4 °C under dry conditions.

3. RESULTS AND DISCUSSION

3.1. Characterization of NCNF Films. Scanning electron microscopy (SEM) and high-resolution transmission electron microscopy (HRTEM) were employed to characterize the NCNF films. As shown in Figure 1A,B, NCNFs exhibited a

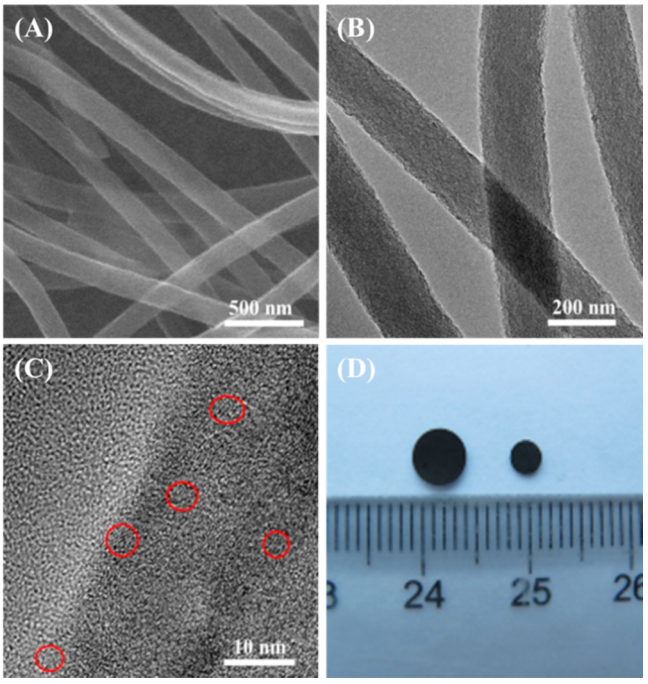

Figure 1. SEM (A), TEM (B), and HRTEM (C) of NCNFs and the photograph of disk-shaped NCNF film (D).

rough surface with an average diameter of 146 nm (n = 20, RSD = 9.5%). Compared with CNFs, obvious morphology changes were observed on NCNFs which displayed smaller diameter and rougher surface (Figure S1A, Supporting Information). These results could be ascribed to the fact that the tail gas, mainly NH_3, would etch the surface of the nanofibers and introduce the N atoms into the carbon during the thermal treatment.[28] Nano-order structures were also observed in the HRTEM image of NCNFs according to Figure 1C. More importantly, NCNFs intercrossed each other and led to the formation of free-standing porous film with high flexibility, and the NCNF film could be easily cut to the disk shape for the modification of the electrode (Figure 1D).

It is accepted extensively that the introduction of heteroatoms into the carbon nanomaterials would yield more

dx.doi.org/10.1021/am501713g | ACS Appl. Mater. Interfaces 2014, 6, 6275−6280

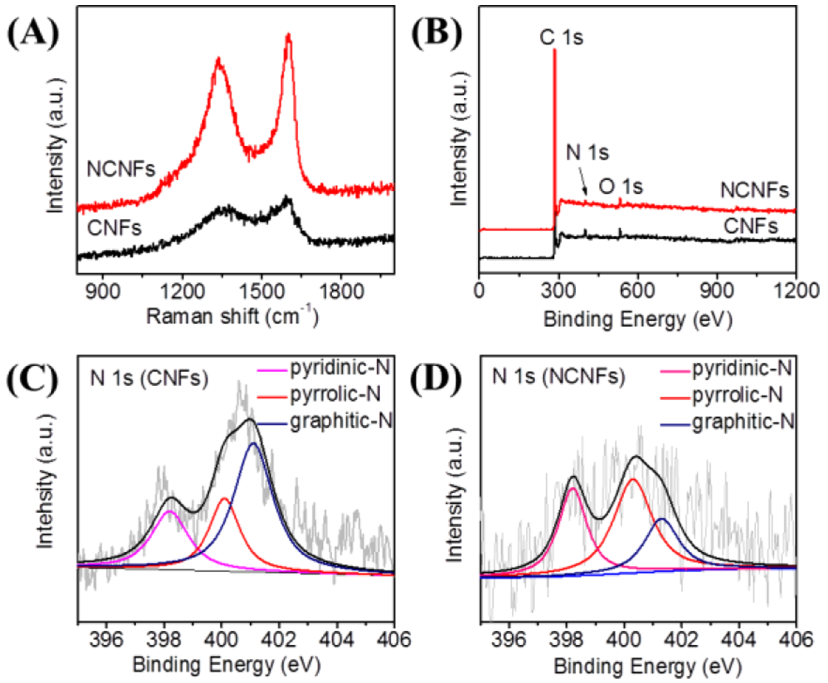

Figure 2. Raman spectrum (A) and XPS spectrum (B) of CNFs and NCNFs and the N 1s spectra of CNFs (C) and NCNFs (D).

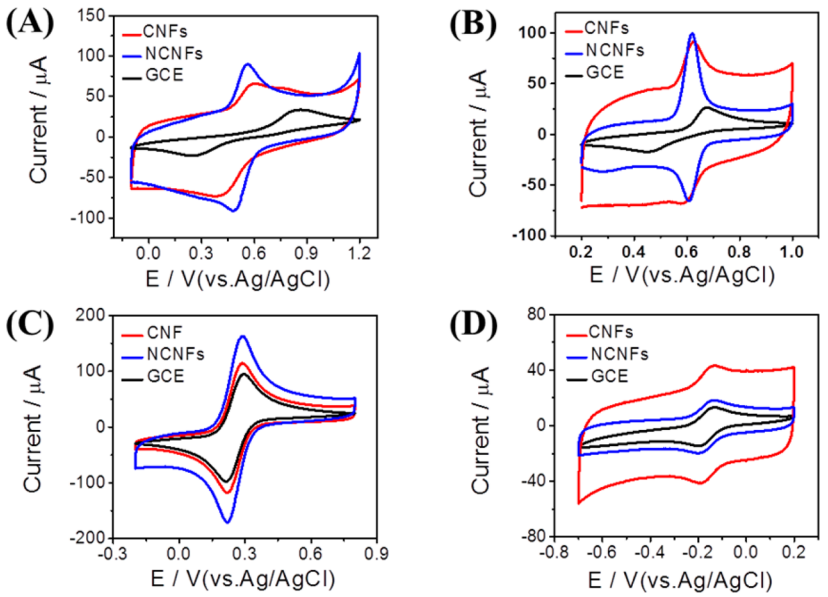

Figure 3. CVs of CNFs/GCE and NCNFs/GCE in 1.0 mM $[Fe(H_2O)_6]^{3+/2+}$ in 0.1 M $HClO_4$ (A), 0.1 mM DA in 0.1 M $HClO_4$ (B), 1.0 mM $[Fe(CN)_6]^{3-/4-}$ in 1.0 M KCl (C), and 1.0 mM $[Ru(NH_3)_6]^{3+/2+}$ in 1.0 M KCl (D), respectively. Scan rate: 50 mV s^{-1}.

defective sites on the surface.[26] In this work, the Raman results demonstrated that the I_D/I_G value of NCNFs (I_D/I_G = 1.942) was larger than that of CNFs (I_D/I_G = 1.850), indicating more defective sites on NCNFs which is in agreement with previous reports (Figure 2A). X-ray photoelectron spectra (XPS) results reveal that the content of nitrogen in NCNFs is smaller than that in CNFs (Figure 2B). However, previous studies demonstrate that the properties of nitrogen-doped carbons, such as catalytic activity, were not directly related to the nitrogen content.[29] The form of N in NCNFs and CNFs was further investigated by N 1s XPS (Figure 2C,D). Generally, the N doped in the carbons is always in the form of pyridinic-N (398.7 ± 0.3 eV), pyrrolic-N (400.4 ± 0.3 eV), and graphitic-N (401.4 ± 0.3 eV).[27,30] According to the N 1s XPS, the content of pyrrolic-N (at. %) in NCNFs and CNFs is 42% and 23%, respectively. It is worthy to note that carbons with pyrrolic-N at the edges of graphene layers would show higher charge mobility and better donor−acceptor properties than pyridinic-N and graphitic-N.[31] Hence, NCNFs may be expected to display a better electrochemical performance relative to CNFs.

For the electrode modification, the NCNF film was cut to the disk shape with the diameter of 2 mm and directly adhered to the surface of the glassy carbon electrode (NCNFs/GCE). Apparently, the modification process of NCNF film is rather simple, and more importantly this could efficiently improve the reproducibility of electrochemical performance at NCNF-based

dx.doi.org/10.1021/am501713g | ACS Appl. Mater. Interfaces 2014, 6, 6275−6280

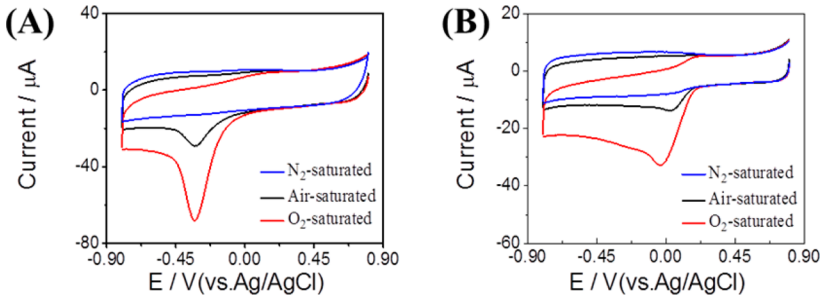

Figure 4. Cyclic voltammograms of CNFs/GCE (A) and NCNFs/GCE (B) in nitrogen-saturated, air-saturated, and oxygen-saturated 0.1 M PBS (pH 7.0), respectively. Scan rate: 50 mV s^{-1}.

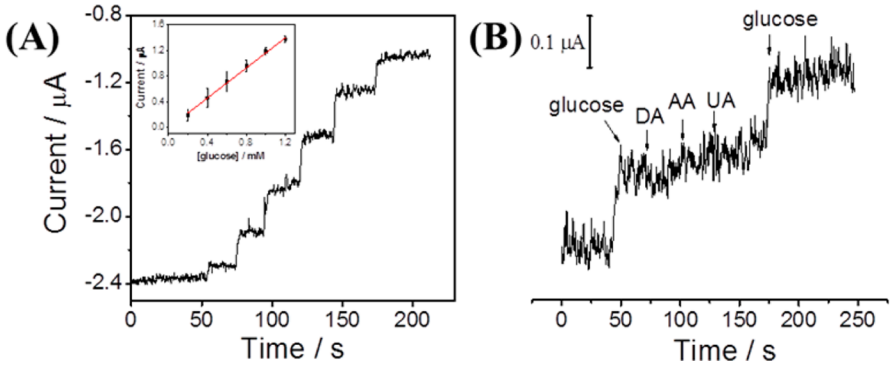

Figure 5. Current−time response curves for successive addition of 0.1 M glucose into the stirred 0.1 M PBS (pH 7.0) under −0.42 V at GOx/NCNFs/GCE. Inset: calibration curves for glucose obtained at GOx/NCNFs/GCE (A). Current−time response curves for addition of 0.4 mM glucose, 1 mM DA, 1 mM AA, 1 mM UA, and 0.4 mM glucose into the stirred 0.1 M PBS (pH 7.0) under −0.42 V at the GOx/NCNFs/GCE(B).

biosensors. To evaluate the electrochemical activity of NCNFs and CNFs, cyclic voltammograms were applied to the redox species $[Ru(NH_3)_6]^{3+/2+}$, $[Fe(CN)_6]^{3-/4-}$, $[Fe(H_2O)_6]^{3+/2+}$, and DA at CNFs/GCE and NCNFs/GCE. Figure 3A shows the cyclic voltammograms of $[Fe(H_2O)_6]^{3+/2+}$ at CNFs/GCE and NCNFs/GCE. Previous reports reveal that the redox species of $[Fe(H_2O)_6]^{3+/2+}$ is sensitive to the presence of surface oxides on the carbon electrode.[32] The peak separation (ΔE_p) is 85 mV at NCNFs/GCE which is much smaller than the value obtained at CNFs/GCE (ΔE_p = 208 mV), indicating a faster electron transfer rate for $[Fe(H_2O)_6]^{3+/2+}$ at NCNFs/GCE. The reason could be attributed to a higher amount of surface oxides at NCNFs.[32] As shown in Figure 3B, the value of ΔE_p for DA also showed an obvious decrease at NCNFs/GCE compared with that at CNFs/GCE. This result could be explained by the rough surface of NCNFs which leads to a larger surface area in comparison with CNFs since the adsorption of DA onto the electrode surface is essential for fast electron transfer. The ΔE_p values observed for $[Fe(CN)_6]^{3-/4-}$ (Figure 3C), which is reported to be sensitive to the surface state, and $[Ru(NH_3)_6]^{3+/2+}$, which is an outer-sphere-type redox species (Figure 3D), were almost unchanged at CNFs/GCE and NCNFs/GCE.[1] On the basis of the results above, NCNFs have a rapid electron transfer rate for the redox probes sensitive to the surface oxide and area.[33]

Previous investigations demonstrate the excellent electrocatalytic performance of nitrogen-doped carbon nanomaterials toward oxygen reduction.[17] Here, we also estimated the oxygen reduction activity at NCNFs and CNFs. Figure 4 shows the cyclic voltammograms of CNFs/GCE (A) and NCNFs/GCE (B) in nitrogen-saturated (blue curve), air-saturated (black curve), and oxygen-saturated (red curve) 0.1 M PBS solution (pH 7.0). The CNFs/GCE and NCNFs/GCE both showed obvious electrocatalytic performance toward oxygen reduction. However, the peak for the oxygen reduction is located at −0.034 V for NCNFs/GCE in oxygen-saturated PBS solution and at −0.330 V for CNFs/GCE. Apparently, NCNFs display higher electrocatalytic activity for the oxygen reduction in comparison with CNFs, which could be attributed to the nitrogen doping and abundant surface defective sites.[34]

3.2. Electrochemical Performance of GOx/NCNFs/GCE. The electrochemical performance of GOx/NCNFs/GCE in nitrogen-saturated 0.1 M PBS (pH 7.0) was investigated. A pair of well-defined redox peaks located at −0.400 and −0.445 V was observed at GOx/NCNFs/GCE (Figure S2, Supporting Information). Although previous reports propose that the voltammetric peaks may be attributed to the redox of flavin adenine dinucleotide rather than the direct electron transfer between GOx and electrode, the small peak separation (ΔE_p = 0.045 V) infers a fast electron transfer rate at NCNFs.[35,36]

The Nyquist plots were measured employing $[Fe(CN)_6]^{3-/4-}$ as the electrochemical probe. As shown in Figure S3 (Supporting Information), the electron transfer resistance at NCNFs/GCE (curve b) was much smaller than that at GCE (curve a), suggesting an outstanding electron transfer activity of NCNFs. Due to the fact that GOx absorbed on the GCE would block the electron exchange between the electrochemical probe and the electrode, a significant increase of resistance was observed on the GOx/GCE (not shown here). However, GOx/NCNFs/GCE (curve c, Figure S3, Supporting Information) exhibited a small resistance for the enhancement of the electron transfer from the NCNFs.

3.3. Glucose Biosensing. Due to their high electrocatalytic activity toward oxygen reduction reaction, the NCNFs could be

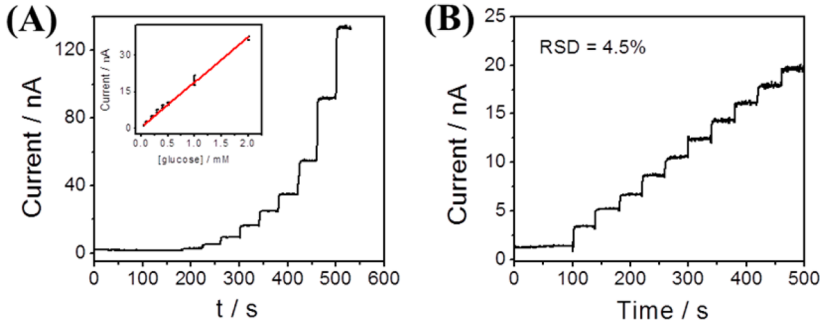

Figure 6. Current−time response curves for the successive addition of 0.1 M glucose into the stirred 0.1 M PBS (pH 7.0) with the working potential of 0.40 V at GOx/NCNFs/GCE (A). Inset: Calibration curves for glucose obtained at GOx/NCNFs/GCE. The current−time response curves for the successive addition of glucose (B).

suitable for the fabrication of a glucose biosensor. Figure 5 presents the amperometric response of the GOx/NCNFs/GCE obtained through injecting sequentially at regular intervals into the continuously stirred PBS (pH 7.0) with an applied electrode potential of −0.42 V. The steady-state current attained 95% within 3 s after the addition of glucose, indicating a fast electron transfer rate and quick response. The inset of Figure 5 illustrates the calibration curve of the response current against the glucose concentration. The performance of this biosensor is shown as follows: linear response range from 0.2 to 1.2 mM with a correlation coefficient of 0.998 and a limit of detection of 0.06 mM (S/N = 3). The as-prepared biosensor exhibits better detection performance compared with the porous CNF/ionic liquid/chitosan composite and MWCNT-coated electrospun gold fibers.[37,38] Besides, the GOx/NCNFs/GCE showed high stability toward the glucose with a relative standard deviation (RSD) of 8.2% for six continuous assays. The influence of interfering species on this biosensor was also measured which shows that 1 mM DA, UA, or AA showed no interference glucose detection, indicating a high selectivity (Figure 5B).

The NCNF was also found to exhibit high catalytic activity for H_2O_2 oxidation (not shown here). To further study the analysis performance of NCNFs, we performed the glucose detection at GOx/NCNFs/GCE with the applied electrode potential of 0.40 V. As shown in Figure 6A, the amperometric response of GOx/NCNFs/GCE was obtained through injecting sequentially at regular intervals into the continuously stirred 0.1 M PBS (pH 7.0). The linear range for the glucose detection was 0.05−3 mM with a correlation coefficient of 0.998, and the detection limit was 0.015 mM (S/N = 3). It displayed high stability toward glucose with a RSD of 4.5% for 10 continuous assays of 0.1 mM glucose (Figure 6B). However, the selectivity toward glucose at 0.40 V at GOx/NCNFs/GCE is relatively poor such that the addition of 0.25 μM AA and UA would affect the detection of 0.5 mM glucose (not shown here). This result, on the other hand, reveals the high electrocatalytic activity of NCNFs.

4. CONCLUSION

In summary, we have proposed a novel method for the simple but efficient preparation of NCNF film and further explored the electrochemical performance of the obtained nanomaterials. The resultant NCNF film exhibits good processabilty originating from the unique free-standing structure and high flexibility. Electrochemical measurements demonstrated that the NCNFs have a fast electron transfer rate and high electrocatalytic activity toward oxygen reduction, which could be attributed to the presence of abundant defective sites and high content of pyrrolic-N on the surface of NCNFs according to the Raman and XPS results. Due to the excellent mechanical and electrochemical properties, the NCNF-based biosensor could be constructed conveniently and realize the glucose detection with high sensitivity and stability. Our work suggests that the free-standing NCNF film could be a suitable platform for high-performance electrochemical biosensors.

■ ASSOCIATED CONTENT

Supporting Information

Figures S1−S3. This material is available free of charge via the Internet at http://pubs.acs.org.

■ AUTHOR INFORMATION

Corresponding Author

*E-mail: youty@ciac.jl.cn.

Notes

The authors declare no competing financial interest.

■ ACKNOWLEDGMENTS

We are grateful for the financial support from NSFC of China (No. 21222505).

■ REFERENCES

(1) McCreery, R. L. Advanced Carbon Electrode Materials for Molecular Electrochemistry. *Chem. Rev.* **2008**, *108*, 2646−2687.

(2) Geim, A. K.; Novoselov, K. S. The Rise of Graphene. *Nat. Mater.* **2007**, *6*, 183−191.

(3) Liao, S. J.; Holmes, K. A.; Tsaprailis, H.; Birss, V. I. High Performance PtRuIr Catalysts Supported on Carbon Nanotubes for the Anodic Oxidation of Methanol. *J. Am. Chem. Soc.* **2006**, *128*, 3504−3505.

(4) Wu, B. H.; Hu, D.; Kuang, Y. J.; Liu, B.; Zhang, X. H.; Chen, J. H. Functionalization of Carbon Nanotubes by an Ionic-Liquid Polymer: Dispersion of Pt and PtRu Nanoparticles on Carbon Nanotubes and Their Electrocatalytic Oxidation of Methanol. *Angew. Chem., Int. Ed.* **2009**, *48*, 4751−4754.

(5) Zhou, M.; Zhai, Y. M.; Dong, S. J. Electrochemical Sensing and Biosensing Platform Based on Chemically Reduced Graphene Oxide. *Anal. Chem.* **2009**, *81*, 5603−5613.

(6) Hao, C.; Ding, L.; Zhang, X. j.; Ju, H. X. Biocompatible Conductive Architecture of Carbon Nanofiber-Doped Chitosan Prepared with Controllable Electrodeposition for Cytosensing. *Anal. Chem.* **2007**, *79*, 4442−4447.

(7) Song, W.; Li, D. W.; Li, Y. T.; Li, Y.; Long, Y. T. Disposable Biosensor Based on Graphene Oxide Conjugated with Tyrosinase

Assembled Gold Nanoparticles. *Biosens. Bioelectron.* **2011**, *26*, 3181−3186.
(8) Sheng, Z. H.; Zheng, X. Q.; Xu, J. Y.; Bao, W. J.; Wang, F. B.; Xia, X. H. Electrochemical Sensor Based on Nitrogen Doped Graphene: Simultaneous Determination of Ascorbic Acid, Dopamine and Uric Acid. *Biosens. Bioelectron.* **2012**, *34*, 125−131.
(9) Guo, H. L.; Peng, S.; Xu, J. H.; Zhao, Y. Q.; Kang, X. F. Highly Stable Pyridinic Nitrogen Doped Graphene Modified Electrode in Simultaneous Determination of Hydroquinone and Catechol. *Sens. Actuator B: Chem.* **2014**, *193*, 623−629.
(10) Zhang, Z. H.; Zhang, R.; Li, C. C.; Yuan, L.; Li, P. P.; Yao, L.; Liu, S. Q. Nitrogen-Doped Carbon Hollow Spheres for Immobilization, Direct Electrochemistry, and Biosensing of Protein. *Electroanalysis* **2012**, *24*, 1424−1430.
(11) Balasubramanian, K.; Burghard, M. Chemically Functionalized Carbon Nanotubes. *Small* **2005**, *1*, 180−192.
(12) Yang, W. R.; Ratinac, K. R.; Ringer, S. P.; Thordarson, P.; Gooding, J. J.; Braet, F. Carbon Nanomaterials in Biosensors: Should You Use Nanotubes or Graphene? *Angew. Chem., Int. Ed.* **2010**, *49*, 2114−2138.
(13) Charlier, J. C.; Terrones, M.; Baxendale, M.; Meunier, V.; Zacharia, T.; Rupesinghe, N. L.; Hsu, W. K.; Grobert, N.; Terrones, H.; Amaratunga, G. A. J. Enhanced Electron Field Emission in B-doped Carbon Nanotubes. *Nano Lett.* **2002**, *2*, 1191−1195.
(14) Florea, L.; Ersen, O.; Arenal, R.; Ihiawakrim, D.; Messaoudi, C.; Chizari, K.; Janowska, I.; Pham-Huu, C. 3D Analysis of the Morphology and Spatial Distribution of Nitrogen in Nitrogen-Doped Carbon Nanotubes by Energy-Filtered Transmission Electron Microscopy Tomography. *J. Am. Chem. Soc.* **2012**, *134*, 9672−9680.
(15) Paraknowitsch, J. P.; Zhang, J.; Su, D. S.; Thomas, A.; Antonietti, M. Ionic Liquids as Precursors for Nitrogen-Doped Graphitic Carbon. *Adv. Mater.* **2010**, *22*, 87−92.
(16) Lee, S. U.; Belosludov, R. V.; Mizuseki, H.; Kawazoe, Y. Designing Nanogadgetry for Nanoelectronic Devices with Nitrogen-Doped Capped Carbon Nanotubes. *Small* **2009**, *5*, 1769−1775.
(17) Gong, K. P.; Du, F.; Xia, Z. H.; Durstock, M.; Dai, L. M. Nitrogen-Doped Carbon Nanotube Arrays with High Electrocatalytic Activity for Oxygen Reduction. *Science* **2009**, *323*, 760−764.
(18) Xu, X.; Jiang, S. J.; Hu, Z.; Liu, S. Q. Nitrogen-Doped Carbon Nanotubes: High Electrocatalytic Activity toward the Oxidation of Hydrogen Peroxide and Its Application for Biosensing. *ACS Nano* **2010**, *4*, 4292−4298.
(19) Xu, X.; Yang, L. J.; Jiang, S. J.; Hu, Z.; Liu, S. Q. High Reaction Activity of Nitrogen-Doped Carbon Nanotubes Toward the Electrooxidation of Nitric Oxide. *Chem. Commun.* **2011**, *47*, 7137−7139.
(20) Wei, W.; Li, P. P.; Li, Y.; Cao, X. D.; Liu, S. Q. Nitrogen-Doped Carbon Nanotubes Enhanced Laccase Enzymatic Reactivity Towards Oxygen Reduction and Its Application in Biofuel Cell. *Electrochem. Commun.* **2012**, *22*, 181−184.
(21) Kamata, T.; Kato, D.; Hirono, S.; Niwa, O. Structure and Electrochemical Performance of Nitrogen-Doped Carbon Film Formed by Electron Cyclotron Resonance Sputtering. *Anal. Chem.* **2013**, *85*, 9845−9851.
(22) Hu, T.; Sun, X.; Sun, H. T.; Yu, M. P.; Lu, F. Y.; Liu, C. S.; Lian, J. Flexible Free-Standing Graphene−TiO_2 Hybrid Paper for Use as Lithium Ion Battery Anode Materials. *Carbon* **2013**, *51*, 322−326.
(23) Feng, D.; Lv, Y. Y.; Wu, Z. X.; Dou, Y. Q.; Han, L.; Sun, Z. K.; Xia, Y. Y.; Zheng, G. G.; Zhao, D. Y. Free-Standing Mesoporous Carbon Thin Films with Highly Ordered Pore Architectures for Nanodevices. *J. Am. Chem. Soc.* **2011**, *133*, 15148−15156.
(24) Liu, C.; Li, F.; Ma, L. P.; Cheng, H. M. Advanced Materials for Energy Storage. *Adv. Mater.* **2010**, *22*, E28−E62.
(25) Liu, Y.; Wang, D. W.; Huang, J. S.; Hou, H. Q.; You, T. Y. Highly Sensitive Composite Electrode Based on Electrospun Carbon Nanofibers and Ionic Liquid. *Electrochem. Commun.* **2010**, *12*, 1108−1111.
(26) Maldonado, S.; Stevenson, K. J. Influence of Nitrogen Doping on Oxygen Reduction Electrocatalysis at Carbon Nanofiber Electrodes. *J. Phys. Chem. B* **2005**, *109*, 4707−4716.
(27) Qiu, Y. J.; Yu, J.; Shi, T. N.; Zhou, X. S.; Bai, X. D.; Huang, J. Y. Nitrogen-Doped Ultrathin Carbon Nanofibers Derived from Electrospinning: Large-Scale Production, Unique Structure, and Application as Electrocatalysts for Oxygen Reduction. *J. Power Sources* **2011**, *196*, 9862−9867.
(28) Wang, X. Q.; Lee, J. S.; Zhu, Q.; Liu, J.; Wang, Y.; Dai, S. Ammonia-Treated Ordered Mesoporous Carbons as Catalytic Materials for Oxygen Reduction Reaction. *Chem. Mater.* **2010**, *22*, 2178−2180.
(29) Reneker, D. H.; Chun, I. Nanometre Diameter Fibres of Polymer, Produced by Electrospinning. *Nanotechnology* **1996**, *7*, 216−223.
(30) Pels, J. R.; Kapteijn, F.; Moulijn, J. A.; Zhu, Q. Evolution of Nitrogen Functionalities in Carbonaceous Materials during Pyrolysis. *Carbon* **1995**, *33*, 1641−1653.
(31) Strelko, V. V.; Kuts, V. S.; Thrower, P. A. On the Mechanism of Possible Influence of Heteroatoms of Nitrogen, Boron and Phosphorus in A Carbon Matrix on the Catalytic Activity of Carbons in Electron Transfer Reactions. *Carbon* **2000**, *38*, 1499−1503.
(32) Chen, P.; Fryling, M.; McCreery, R. L. Electron Transfer Kinetics at Modified Carbon Electrode Surfaces: The Role of Specific Surface Sites. *Anal. Chem.* **1995**, *67*, 3115−3122.
(33) Ueda, A.; Kato, D.; Kurita, R.; Kamata, T.; Inokuchi, H.; Umemura, S.; Hirono, S.; Niwa, O. Efficient Direct Electron Transfer with Enzyme on a Nanostructured Carbon Film Fabricated with a Maskless Top-Down UV/Ozone Process. *J. Am. Chem. Soc.* **2011**, *133*, 4840−4846.
(34) Liang, Y. Y.; Wang, H. L.; Zhou, J. G.; Li, Y. G.; Wang, J.; Regier, T.; Dai, H. J. Covalent Hybrid of Spinel Manganese−Cobalt Oxide and Graphene as Advanced Oxygen Reduction Electrocatalysts. *J. Am. Chem. Soc.* **2012**, *134*, 3517−3523.
(35) Goran, J. M.; Mantilla, S. M.; Stevenson, K. J. Influence of Surface Adsorption on the Interfacial Electron Transfer of Flavin Adenine Dinucleotide and Glucose Oxidase at Carbon Nanotube and Nitrogen-Doped Carbon Nanotube Electrodes. *Anal. Chem.* **2013**, *85*, 1571−1581.
(36) Wooten, M.; Karra, S.; Zhang, M. G.; Gorski, W. On the Direct Electron Transfer, Sensing, and Enzyme Activity in the Glucose Oxidase/Carbon Nanotubes System. *Anal. Chem.* **2014**, *86*, 752−757.
(37) Sheng, Q. L.; Liu, R. X.; Zheng, J. B.; Lin, W. H.; Li, Y. Y. Direct Electrochemistry of Glucose Oxidase Immobilized on Porous Carbon Nanofiber/Room Temperature Ionic Liquid/Chitosan Composite Film and Its Biosensing Application. *J. Solid State Electrochem.* **2012**, *16*, 739−745.
(38) Jose, M. V.; Marx, S.; Murata, H.; Koepsel, R. R.; Russell, A. J. Direct Electron Transfer in a Mediator-Free Glucose Oxidase-Based Carbon Nanotube-Coated Biosensor. *Carbon* **2012**, *50*, 4010−4020.